NMR studies of EuB_6 at low temperatures

B. Ambrosini, J. L. Gavilano, P. Vonlanthen, and H. R. Ott
Laboratorium für Festkörperphysik, ETH-Hönggerberg, CH-8093 Zürich, Switzerland

D. P. Young and Z. Fisk
National Magnetic Field Laboratory, Florida State University, Tallahassee, Florida 32306

(Received 16 February 1999)

We report results of ^{153}Eu and ^{11}B nuclear magnetic resonance (NMR) measurements on EuB_6 at temperatures between 0.1 and 150 K and in external magnetic fields between $H=0$ and 7 T. The evolution of the ^{153}Eu NMR spectra at low temperatures and low fields provides evidence for an unexpected and complex electronic ground state of EuB_6, involving the coexistence of two magnetically very similar phases. The temperature and magnetic-field dependences of the ^{11}B spin-lattice relaxation rate $T_1^{-1}(T,H)$ are very well accounted for by magnon-driven relaxation. A spin-wave theoretical interpretation of the ^{153}Eu-NMR spectra and the ^{11}B T_1^{-1}measurements indicate that a gap of the order of 1 K exists in the magnon excitation spectrum.
[S0163-1829(99)08329-0]

I. INTRODUCTION

Because of its unusual electronic and magnetic properties the cubic compound EuB_6 has now been in the focus of research activities for more than 30 years. Since in this compound the Eu ions adopt a divalent configuration, EuB_6 was initially thought to be a magnetic semiconductor.[1] However, more recent resistivity results definitely imply a semimetallic character below 300 K with a very low charge-carrier concentration.[2,3] This interpretation is supported by self-consistent band-structure calculations indicating a small band overlap at the X point of the Brillouin zone.[4]

At low temperatures, EuB_6 orders ferromagnetically[5] via two consecutive phase transitions at $T=16$ and 14 K, respectively, as inferred from two anomalies in the temperature dependence of the specific heat.[6,7] The ferromagnetic transition is accompanied by a significant reduction of the resistivity ρ and in the temperature range of these transitions, EuB_6 also exhibits a large negative magnetoresistance.[3] The increasingly metallic character of EuB_6 below the Curie temperature T_C is also obvious from the results of optical reflectivity measurements. A considerable blue shift of the reflectivity edge is signaling a strong increase of the unscreened plasma frequency in the ferromagnetic phase.[6] The electrical resistivity also shows a large reduction with increasing pressure, concomitant with an increase of the magnetic phase-transition temperature. These results have been claimed to indicate a Ruderman-Kittel-Kasuya-Yosida-type coupling between the Eu moments via the conduction electrons.[8]

A very detailed study of the magnetic behavior, reported in Ref. 7, has been made in the temperature range of the two ferromagnetic transitions by means of measurements of the magnetization and the magnetic susceptibility. From these results it has been argued that in the magnetically ordered phase found between $T\approx 16$ and 14 K the moments are ferromagnetically aligned along the [100] direction and that the phase transition at $T\approx 14$ K corresponds to a moment reorientation from the [100] to the [111] direction. In addition the behavior of the low-temperature resistivity has been claimed to reflect the opening of a gap of $E_g/k_B=\Delta=45$ K in the magnon excitation spectrum.

In order to etablish a more extended database with microscopic information for a reliable interpretation of the intriguing features of EuB_6, we have made a number of NMR measurements on both ^{153}Eu and ^{11}B nuclei, at temperatures between 0.1 and 150 K and in external magnetic fields H between 0 and 7 T. For comparison, also NMR spectra and spin-lattice relaxation rate measurements have been made on the related nonmagnetic metallic hexaboride LaB_6.

After giving some details concerning the samples and the experimental procedures in Sec. II, we present and discuss our results in Sec. III. We first display the results of the NMR spectra and spin-spin relaxation rate measurements on the isotope ^{153}Eu in Secs. III A–III C. Subsequently, the ^{11}B-NMR spectra and the corresponding spin-lattice relaxation rate measurements on EuB_6 and LaB_6 are discussed in Secs. III D and III E. In Sec. IV we offer some conclusions that follow from this study. Part of our NMR results on ^{153}Eu presented here have previously been published elsewhere.[9,10]

II. SAMPLE AND EXPERIMENT

A. Sample

The hexaboride material used in our NMR investigation was grown in the form of small single crystals by melting the appropriate amounts of the pure elements in aluminum flux. After the thermal treatment the crystals were separated from the Al in a hot NaOH solution.[2,6] Hexaboride samples prepared by this method have been shown to be of very high quality in structural perfection and chemical composition.[11] For our experiments the crystals have been powdered in an argon atmosphere to grains with a typical size of less than 100 μm.

B. Experiment

The NMR measurements below 4 K were performed in a dilution ^{3}He-^{4}He refrigerator, where the powdered sample

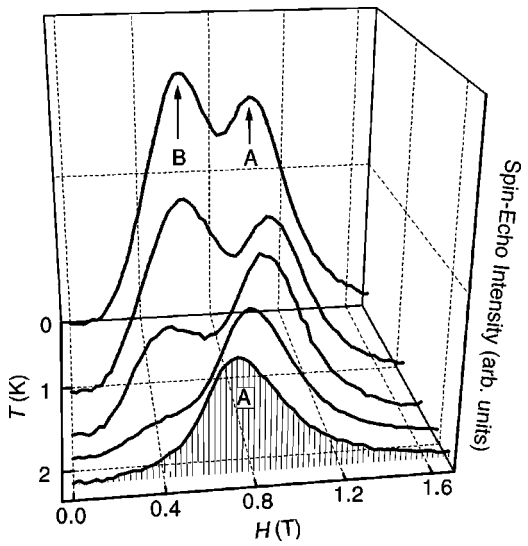

FIG. 1. ^{153}Eu-NMR spectra for EuB_6 measured at various temperatures and a fixed frequency of 156.36 MHz. The data below 2 K show two broad peaks (A and B).

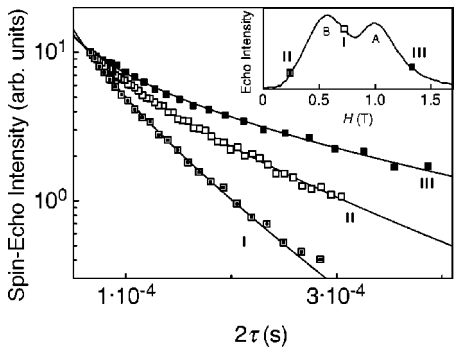

FIG. 2. Echo-decay curves of ^{153}Eu in EuB_6 at 1.1 K measured in applied magnetic fields of 0.24 (I), 0.72 (II), and 1.33 T (III). The solid lines represent the best fits to the data as described in the text. The inset shows the ^{153}Eu-NMR spectrum for $T=1.1$ K with the symbols placed where the corresponding spin-echo decays have been measured.

was kept in contact with the liquid ^{3}He-^{4}He mixture. For the measurements above 4 K the specimens were kept in flowing He gas.

In all our measurements the NMR signal intensity was obtained by integrating the spin-echo signal. The NMR spectra were collected at constant frequency or field by stepwise varying the applied magnetic field or the irradiation frequency, respectively. The measurements of the spin-lattice relaxation times T_1 involved the monitoring of the nuclear magnetization recovery $m(t)$ of ^{11}B as a function of the time delay after the application of a single rf pulse or a comb of rf pulses.

The spin-spin relaxation time T_2, measured for EuB_6 on the ^{153}Eu isotope, was obtained by monitoring the spin-echo intensity as a function of the time delay between the pulses.

III. RESULTS AND DISCUSSION

A. ^{153}Eu-NMR spectra

In Fig. 1 we display examples of ^{153}Eu-NMR spectra of EuB_6 between 0.08 and 2.15 K, measured at a fixed frequency of 156.36 MHz. Above 2 K the spectrum consists of a single broad line A, but as the temperature is reduced to below 2 K a second line B at a lower field appears and gradually gains in relative intensity at the expense of line A (see Fig. 1). Below 1.1 K the relative intensity of signal B saturates at approximately the same level as signal A.

The appearence of two peaks in the NMR spectrum of ^{153}Eu is unexpected because the occurrence of inequivalent magnetic sites in a simple cubic structure like that of EuB_6 cannot *a priori* be anticipated. Two scenarios may, nevertheless, be postulated that could lead to this unexpected behavior: (a) inequivalent Eu sites in a single phase or (b) the coexistence of two different phases.

The existence of two inequivalent Eu sites in the same magnetic phase seems very unlikely. In general even a temperature-induced lowering of the crystal symmetry by lattice distortion yields a single site and hence a single-peak NMR signal. Our observations show that the shifts of the maxima of signals A and B are both proportional to the temperature dependence of the bulk magnetization. It seems rather unlikely that a lowering of the symmetry that results in two different sites, leaves the hyperfine field associated with the high-temperature phase essentially unchanged. Still assuming such a scenario to be possible, one would rather expect the single peak to progressively separate into two peaks corresponding to the two inequivalent sites. Our observation, however, shows that peak B does not separate from peak A but rather appears at a different field. A scenario considering different hyperfine fields due to two crystal-field split *f*-electron states, only slightly separated in energy, is not compatible with our observation of two almost equally intense lines even at the lowest temperatures. Therefore, we conclude that our results for the NMR spectra are most likely caused by the coexistence of two different phases at low temperatures.

The maxima of signals A and B shown in Fig. 1 correspond, below 1.1 K, to hyperfine fields $H_{\rm hf}$ at the Eu nuclei of -34.54 and -34.18 T, respectively. The negative sign indicates that the hyperfine fields are oriented antiparallel to the applied magnetic field, as expected for a dominant core polarization contribution to the hyperfine field. The difference between the average hyperfine fields of line A and B is of the order of 1%. This small difference rules out any significant valence change of a good part of the Eu^{2+} ions as the origin for the unusual behavior indicated by our results.

B. ^{153}Eu-spin-spin relaxation rate

In Fig. 2 we present typical ^{153}Eu spin-echo decay curves of EuB_6 measured at 156.36 MHz and $T=1.1$ K in three different fields. The labeling of the curves by I, II, and III denotes three magnetic fields which are also displayed on the profile of the corresponding NMR spectrum in the inset of the same figure. The echo intensities have been normalized to have the same value at the shortest possible time of monitoring. Technical limitations and very short spin-spin relaxation times T_2 allowed us to measure only the tail end of the echo-decay curve. The decay is nonexponential in time, suggesting an inhomogeneous distribution of T_2's.

In previous work Barak and co-workers[12] proposed a model for describing the spin-spin relaxation in ferromagnetic systems where the broadening of the NMR signals is due to microscopic and macroscopic inhomogeneities. In this model the relaxation mechanism is provided by the indirect Suhl-Nakamura (SN) interaction. One can visualize this effective coupling between two nuclear spins by considering that a spin-flip of say, nuclear spin 1, creates a virtual magnon in the ferromagnetic background. This virtual magnon may then be annihilated by a spin-flip of the nuclear spin 2, hence leading to an effective spin-spin interaction.

In real ferromagnetic systems, microscopic imperfections like strains or impurities cause the local magnetic field to vary from site to site. In a first approximation, the resultant microscopic distribution of Larmor frequencies is assumed to be the same throughout the whole sample, being approximated by a function of the form $g(\nu-\nu_0)$, where ν_0 represents the mean frequency of the microscopic domain. Consider now a spin i and its neighbors, arranged in shells labeled with index j. If the characteristic width of the Zeeman energy distribution given by $g(\nu-\nu_0)$ is larger than the effective SN coupling constant between spin i and a spin in the jth shell, then the SN interaction will spin-flip only a fraction of the nuclear spins in the jth shell, resulting in an increase of the spin-spin relaxation time. The relaxation rate $T_2^{-1}$for a given microscopic region, characterized by $g(\nu-\nu_0)$, will depend on the Larmor frequency as

$$T_2^{-1}(\nu)=Cg(\nu-\nu_0), \tag{1}$$

where C is a constant independent of ν. In real ferromagnets the width of the NMR signals is expected to be much larger than (i) the width of the microscopic distribution $g(\nu-\nu_0)$ and, (ii) the characteristic irradiation width γH_1 of the rf pulse. In this case the integrated intensity $m_\perp(t)$ of the spin echo, as a function of the time delay t between the pulses, is expected to be nonexponential with

$$m_\perp(t)\propto\int_{-\infty}^{\infty}g(\nu')e^{-t([1/T_2^{(0)}]g(\nu'))}d\nu', \tag{2}$$

where $\nu'=\nu-\nu_0$ and $T_2^{(0)}\equiv T_2(\nu=\nu_0)$ as given in Eq. (1). In what follows, we will denote the fit parameter $T_2^{(0)}$ simply as T_2. We have used Eq. (2) to fit our measured echo-decay data with only two parameters, i.e., T_2 and an overall scaling factor, absorbing the width and the amplitude of $g(\nu')$. As previously experienced by Barak and co-workers,[12] the best fits to the data are obtained using a Lorentzian distribution of microscopic frequencies $g(\nu-\nu_0)$. The solid lines in Fig. 2 represent the best fits to our measurements.

In Fig. 3 we display the field dependence of T_2^{-1} at 5 different temperatures between 0.08 and 1.82 K, measured at $\nu=156.36$ MHz. In the inset of the same figure we compare the NMR spectrum and the corresponding $T_2^{-1}(H)$ measured at 0.08 K. We now intend to demonstrate that, although these measurements have only been possible at the tail ends of the echo-decay envelope $m_\perp(t)$, our results reflect intrinsic properties of EuB_6 and are not artifacts due to the experimental limitations. Below we offer some general considerations and several simulations that support our interpretation.

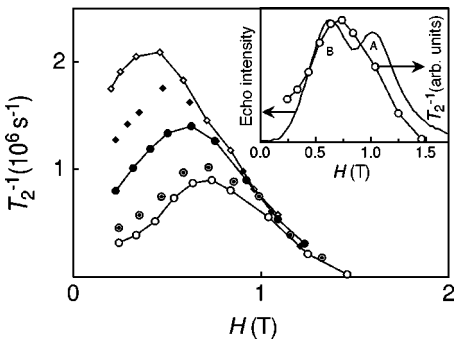

FIG. 3. T_2^{-1} as a function of the applied field for ^{153}Eu in EuB_6, measured at 156.36 MHz and temperatures (from top to bottom) of 1.82, 1.65, 1.47, 1.1, and 0.08 K. The solid lines are to guide the eye. The inset shows the ^{153}Eu-NMR spectrum and the corresponding T_2^{-1} profile for $T=0.08$ K. Note that the minimum of the spectrum does not coincide with the maximum of T_2^{-1}.

First of all, the model employed to analyze the echo-decay curves is based on reasonable assumptions and has successfully been used in the past to analyze similar data on related ferromagnets.[12] Our estimated values of T_2^{-1} are in qualitative agreement with the measured curves, i.e., a visibly faster relaxation corresponds to a larger T_2^{-1} (see Fig. 2). As may be seen in the inset of Fig. 3, T_2^{-1} is not constant across the NMR spectrum and therefore its shape may be affected by T_2^{-1}effects. However, from the measured echo-decay envelopes along the profile of the NMR signal we can, via Eq. (2), estimate the NMR spectrum at zero delay between the pulses. An example of such a reconstructed signal compared with the corresponding measured spectrum is shown in Fig. 4. It is obvious that the two-peak feature is preserved and that only the relative intensity of the two peaks is affected. The slight shift in magnetic field of ~ 0.05 T between the maxima of peak A of the experimental and the reconstructed curve is insignificant if we consider the magnitude of the hyperfine field of the order of 30 T. As a test of confidence of this procedure we have calculated the product of the reconstructed spectrum intensity $\mathcal{A}$ multiplied

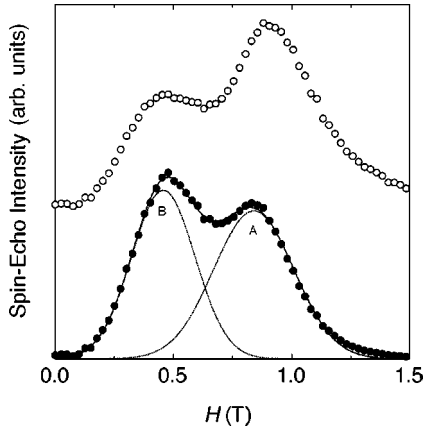

FIG. 4. ^{153}Eu-NMR spectrum for EuB_6 measured at $T=1.65$ K and $\nu=156.36$ MHz (open circles). The full circles represent the reconstructed spectrum for a zero delay between the pulses (see text). The solid line represents the best fits to the data assuming the two Gaussian functions shown by the dotted lines.

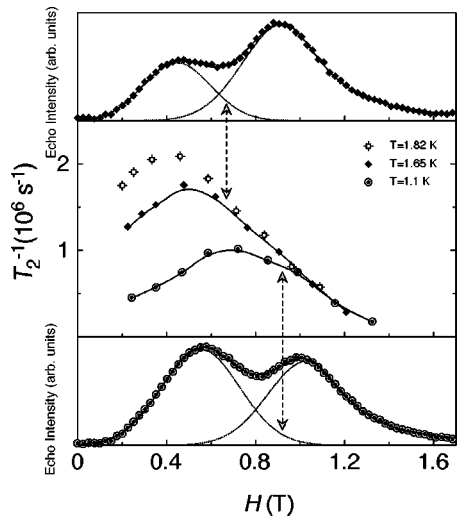

FIG. 5. ^{153}Eu-NMR spectra for EuB_6 measured at 1.1 and 1.65 K (symbols in the lower and upper figure, respectively). The dotted lines represent a tentative estimate of line A and B in the overlapping region. In the central figure we display the field dependence of T_2^{-1}. Note that the deviation of T_2^{-1} from the high-field *T*-independent region approximately corresponds to the onset of line B. The data at $T=1.82$ K are included to demonstrate the crossover of the measured T_2^{-1} at 1.65 K from the *T*-independent to the *T*-dependent region.

by the temperature *T*. For temperatures between 1 and 2 K where signal B decreases from its saturation value and finally vanishes, the product $\mathcal{A}\cdot T$ is found, as expected, to be temperature independent with an uncertainty of less than 10%. This result represents a strong quantitative support for the reliability of our approach.

In Fig. 3 we observe that in fields exceeding 0.9 T, where signal A is dominant for all the chosen temperatures, $T_2^{-1}$is approximately *T* independent and increases with decreasing field. With further decreasing field, entering the range where peak B starts dominating, T_2^{-1}acquires a significant temperature dependence. Thus, $T_2^{-1}(H)$ reaches a maximum, whose position and magnitude now depends on temperature, and decreases with decreasing field at fields where peak B is in the dominant part of the spectrum. In Fig. 5 we attempt to demonstrate that the onset of the *T* dependence of $T_2^{-1}(H)$ more or less coincides with the onset of signal B in the NMR spectrum. This behavior, once again, indicates that the two-peak feature is not an experimental artifact.

In Fig. 6 we display the relative intensity of peak B of reconstructed spectra as a function of temperature. It may be seen that signal B vanishes at approximately 2 K. In Fig. 7 we present the temperature dependence of T_2^{-1} estimated at 0.3 Tesla (full circles) and at 1.18 T (open circles), two fields at which peak B and peak A, respectively, have been shown to be dominant in this temperature range. At these fields, $T_2^{-1}$is *T* independent for peak A, whereas it increases rapidly as the temperature is enhanced towards 2 K for peak B, giving evidence that signals A and B are associated with two coexisting phases and not with different sites in a single phase. A comparison of Figs. 6 and 7 shows that the increase and perhaps the divergence of T_2^{-1}approximately scales in temperature with the progressive disappearance of peak B. In conclusion, the features of Figs. 6 and 7 of the ^{153}Eu-NMR

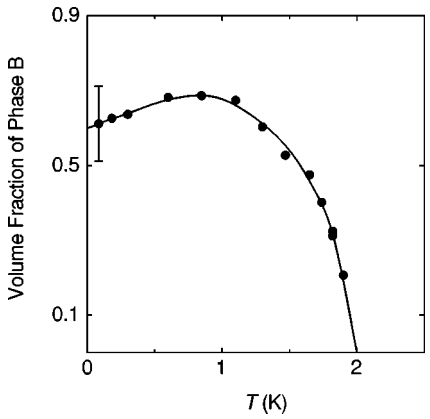

FIG. 6. Temperature dependence of the relative NMR integrated intensity of peak B in the reconstructed spectrum (see text). The solid line is to guide the eye.

measurements indicate that the observed unusual features are associated with a critical behavior of phase B.

C. Magnetization

In Fig. 8 we display the temperature dependence of the frequency at which peak A is maximum in a constant external field $H=1$ T. The resonance frequency at the magnetic site of a ferromagnet can be expressed as a sum of four terms[13]

$$\nu=\frac{\gamma}{2\pi}\left|H-D_{\mathrm{f}}\mu_0 M+\frac{\mu_0}{3}M+H_{\mathrm{hf}}\frac{M}{M_0}\right|, \tag{3}$$

where *H* is the applied field. The second and the third term represent the demagnetization and the Lorentz field, respectively, with D_{f} being the demagnetization factor. Our measurements were made on powdered EuB_6. For simplicity we assume an average $D_{\mathrm{f}}=1/3$, implicitly implying an ''average spherical geometry'' of our grains. Hence, the Lorentz and the demagnetization field cancel each other. The last term of Eq. (3) represents the hyperfine field. Except for the applied field, all the contributions to $\nu(T)$ are proportional to the

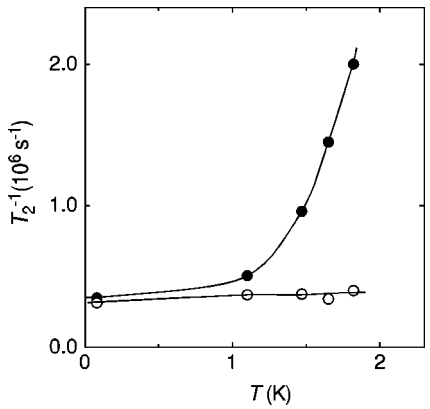

FIG. 7. Temperature dependence of T_2^{-1} estimated at 0.3 T (full circles) and at 1.18 T (open circles), two fields at which line B and line A, respectively, are dominant in this temperature range. The measurements were performed at 156.36 MHz. The solid lines are to guide the eye.

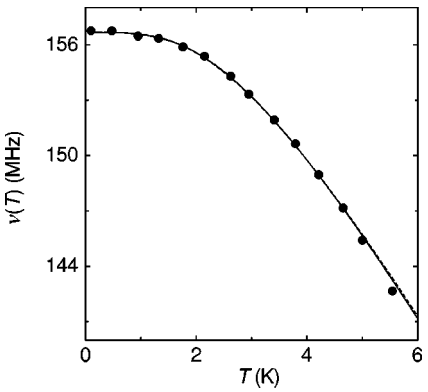

FIG. 8. Temperature dependence of the frequency at which peak A is maximum measured in an external field of 1 T (full circles). The solid and broken lines represent simulations of $\nu(T)$ according to the spin-wave theory (see text) for $J_1=J_2=0.063$ K and $\Delta=0$ K and for $J_1=0.157$ K, $J_2=0$ and $\Delta=1.4$ K, respectively, (note that for simplicity we write J_n but mean J_n/k_B).

magnetization $M(H,T)$. Since for the data shown in Fig. 8, H represents only a small fraction of about 3% of H_{hf}, plotting $\nu(T)$ is obviously a very useful way to establish the temperature variation of the magnetization.

At sufficiently low temperatures the spin-wave approximation for describing the ferromagnetic state can be applied. In our analysis of the temperature dependence of the resonance frequency $\nu(T)$ of the ^{153}Eu nuclei we essentially rely on the theoretical scheme developed by Holstein and Primakoff (HP).[14] The Hamilton operator describing the system contains in addition to the exchange term a Zeeman and a dipole-dipole interaction and may be written as

$$\mathcal{H}_{HP}=-\sum_{i,j} J_{ij}\mathbf{S}_i\cdot\mathbf{S}_j-g\mu_B H\sum_i \mathbf{S}_i^z+\frac{\mu_0(g\mu_B)^2}{4\pi}\times\sum_{i,j}\left(\frac{\mathbf{S}_i\cdot\mathbf{S}_j}{r_{ij}^3}-\frac{3(\mathbf{S}_i\cdot\mathbf{r}_{ij})(\mathbf{S}_j\cdot\mathbf{r}_{ij})}{r_{ij}^5}\right), \tag{4}$$

where the symbols have their usual meaning. From Eq. (4) we obtain the magnetization

$$M(H,T)=M_0-M_T(H,T)-M_\beta(H). \tag{5}$$

Here, M_T represents the deviation from the saturation value M_0 due to thermal excitations. It is given by

$$M_T(H,T)=\frac{g\mu_B}{V}\sum_{\mathbf{k}}\frac{A_{\mathbf{k}}}{\epsilon_{\mathbf{k}}}\frac{1}{\exp(\epsilon_{\mathbf{k}}/k_BT)-1} \tag{6}$$

with V being the volume. In Eq. (5) M_β is a T-independent term associated with the dipole-dipole interaction

$$M_\beta(H)=\frac{g\mu_B}{2V}\sum_{\mathbf{k}}\left(\frac{A_{\mathbf{k}}}{\epsilon_{\mathbf{k}}}-1\right). \tag{7}$$

The spin-wave parameters $\epsilon_{\mathbf{k}}$, $A_{\mathbf{k}}$ and $B_{\mathbf{k}}$ are defined as

$$\epsilon_{\mathbf{k}}=\sqrt{A_{\mathbf{k}}^2-B_{\mathbf{k}}^2}, \tag{8}$$

$$A_{\mathbf{k}}=g\mu_B H-\frac{3}{2}D_f\mu_0 g\mu_B M+2S\sum_{\mathbf{n}} J_n(1-e^{i\mathbf{k}\cdot\mathbf{r}_n})+B_{\mathbf{k}}, \tag{9}$$

and

$$B_{\mathbf{k}}=\frac{1}{2}g\mu_B\mu_0 M\sin^2\theta_{\mathbf{k}}, \tag{10}$$

where $\theta_{\mathbf{k}}$ represents the angle between the magnetization and the spin-wave propagation vector $\mathbf{k}$. J_n is the exchange integral for the nth nearest neighbors. For simplicity we assume that only J_1 and J_2 are different from zero and we neglect the influence of neighbors at larger distances. A gap in the magnon excitation spectrum associated with anisotropy will be considered by adding a term to the external field, defining

$$H\equiv H_{ext}+H_\Delta=H_{ext}+\frac{k_B}{g\mu_B}\Delta. \tag{11}$$

The solid and broken lines in Fig. 8 display the results of simulations of $\nu(T)$ assuming different values of J_1, J_2, and Δ. The best agreement between the result of our measurements and our model calculation is obtained for $J_1=J_2=0.063$ K and $\Delta=0$ K or for $J_1=0.157$ K, $J_2=0$ and $\Delta=1.4$ K (note that for simplicity we write J_n but mean J_n/k_B). In fact from our simulations we cannot distinguish between the cases $\Delta=1.4$ K with $J_1\gg J_2$ and a vanishingly small gap with $J_1\approx J_2\approx 0.063$ K. Even an intermediate situation is possible, because J_2 and Δ have a similar effect on $\nu(T)$. In conclusion the results of our simulations allow us to put an upper limit to any anisotropy gap of a few Kelvin, in agreement with a recent neutron-diffraction result.[5] From J_1 and J_2 we can estimate the transition temperature in a molecular-field approximation[15] (MFA) to be

$$k_BT_c^{MFA}=\frac{2}{3}S(S+1)(z_1J_1+z_2J_2), \tag{12}$$

where $z_1=6$ and $z_2=12$ are the number of nearest and next-nearest Eu neighbors of the Eu sites in EuB_6. In both cases discussed above ($\Delta\approx 0$ or $J_2\approx 0$), the estimated transition temperatures are of the order of 10 K, in fair agreement with T_C established with specific-heat and magnetization measurements.[5–7] A closer agreement cannot be expected because the shape of the specific-heat anomaly[6,7] clearly signals the inadequacy of the MFA for describing the transition.

D. ^{11}B-NMR spectra of EuB_6 and LaB_6

In Fig. 9 we display examples of ^{11}B-NMR spectra for EuB_6, measured at several temperatures and at a fixed frequency of 63 MHz. From NMR measurements on the related compound LaB_6, presented in Fig. 10, we expect the quadrupole splitting of the ^{11}B signal to be of the order of 0.5 MHz, much less than the characteristic width of the ^{11}B-NMR spectrum of EuB_6 at low temperatures. Therefore, the prominent shoulder that appears in the ^{11}B-NMR spectrum of EuB_6 at low temperatures is attributed to differences in the local fields. The low-temperature spectra are well approximated by the sum of two Gaussians, here denoted by I and II, as shown in Fig. 9 for the spectrum taken at T

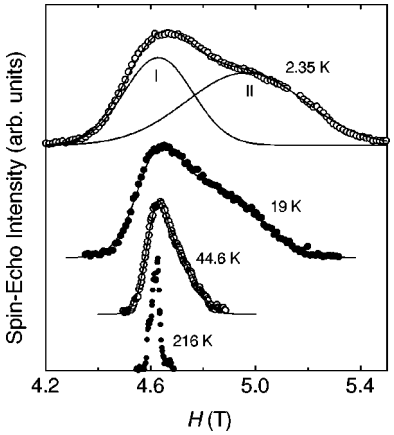

FIG. 9. ^{11}B NMR spectra of EuB_6 between 2.35 and 216 K measured at $\nu = 63$ MHz. The solid lines represent the best fits to the data using two Gaussian functions, as indicated in the top spectrum with I and II.

$=2.35$ K. The individual contributions have integrated intensities of 1/3 and 2/3, respectively. At the lowest measured temperatures the internal static fields $H_{\rm hf}$, obtained from the shift of the center of the Gaussian relative to the expected position of the boron NMR line in a diamagnetic substance, are -0.02 and -0.35 T for the minority (peak I) and majority (peak II) boron sites, respectively.

The observed splitting of the maxima of peak I and II, $\Delta H \approx 0.33$ T, is in good quantitative agreement with the difference of the dipole fields at the B sites obtained by assuming the full Eu^{2+} moments being oriented along the [110] direction. Calculations assuming this orientation result in a direct dipole field $H_d = -0.116$ T at 4 boron sites in the unit cell and $H_d = 0.232$ T at the remaining two sites, thus leading to a difference in field of $\Delta H = 0.348$ T. To reproduce the observed maxima of peak I and II in the NMR spectrum we have to assume an additional hyperfine transferred field due to *f*-electron moments on the Eu ions of ~ -0.24 T. According to Süllow *et al.*,[7] the Eu moments are claimed to be oriented along the [111] direction at low temperatures. This moment arrangement results in a vanishing contribution of the dipole field at all B nuclei and hence, two different

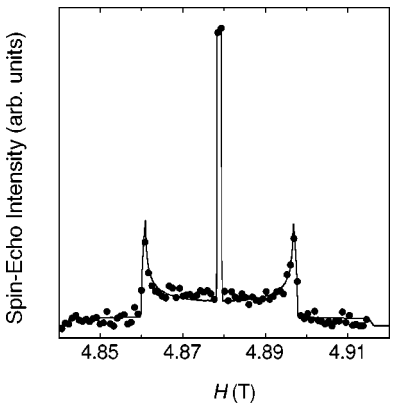

FIG. 10. ^{11}B NMR spectrum of LaB_6 measured at 18 K and $\nu = 66.71$ MHz. The solid line represents the best fit assuming a first-order quadrupole perturbation of a Zeeman interaction dominated powder pattern.

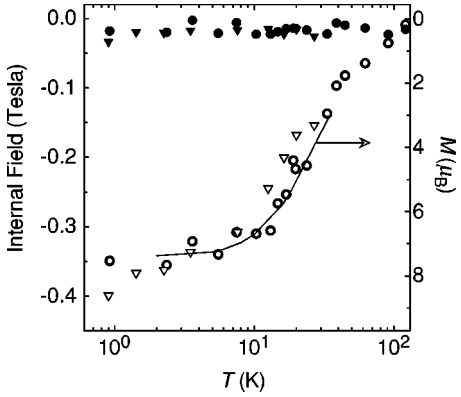

FIG. 11. Temperature dependences of the average hyperfine fields $\langle H_{\rm hf} \rangle$ of line I and II (full and open symbols, respectively) measured at $\nu = 32.5$ MHz (triangles) and $\nu = 63$ MHz (circles). The solid line displays the temperature dependence of the magnetization at $H = 5$ T.

transfer hyperfine fields would be needed to explain our measurements. A hypothetical orientation of the moments along the [100] direction would also produce two inequivalent B sites with a dipole-field difference $\Delta H = -0.7$ T. This situation would require two transferred fields that differ in magnitude and direction, hence implying a strong anisotropic transferred hyperfine coupling for explaining our results. For any of these orientations we cannot exclude that a slight distortion of the crystal lattice is the cause of our observations. At any rate, the temperature dependence of the ^{11}B-NMR spectra does not dramatically change below 3 K and we may, therefore, exclude a moment reorientation or a considerable alteration of electronic densities to be the cause of the appearance of the two inequivalent phases as discussed in Sec. III A

In Fig. 11 we display the temperature dependence of the average hyperfine field $\langle H_{\rm hf} \rangle$ of peaks I and II with full and open symbols, respectively, measured at $\nu = 32.5$ MHz (triangles) and $\nu = 63$ MHz (circles). The solid line displays the temperature dependence of the magnetization of a sample prepared from the same piece of material in a field $H = 5$ T.[16] The T dependence of $\langle H_{\rm hf} \rangle$ for the majority sites II follows the temperature dependence of the bulk magnetization fairly well, indicating that it is a consequence of the magnetic ordering. For the minority boron site I, $\langle H_{\rm hf} \rangle (T)$ is too small to draw any reliable conclusion.

E. ^{11}B spin-lattice relaxation rate in EuB_6 and LaB_6

The ^{11}B T_1 measurements were made near the maximum of the spin-echo intensity (see Fig. 9) and thus have the largest contribution from peak I of the ^{11}B-NMR spectra. In Fig. 12 we display $T_1^{-1}(T)$ measured in applied magnetic fields between 0.49 and 7 T (symbols). The solid lines represent the results of calculations to be discussed below and the dashed line represents $T_1^{-1}(T)$ measured for LaB_6. The spin-lattice relaxation in the range of the spectrum, where the ^{11}B-NMR signal is dominated by peak II, is essentially the same as that for the boron peak I. This implies again that the observed order-of-magnitude difference between the hyperfine fields at the boron sites I and II is the result of cancellations of different contributions to the local fields.

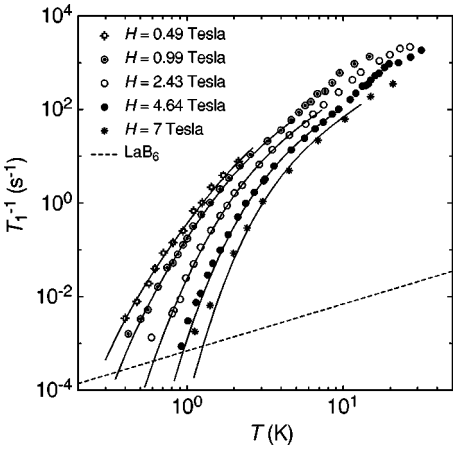

FIG. 12. Temperature dependence of the ^{11}B spin-lattice relaxation rate measured in various magnetic fields from 0.49 to 7 T (symbols). The solid lines represent calculations considering two-magnon-dominated processes at the respective field and assuming an energy gap in the magnon excitation spectrum of 1.4 K (see text).

Except at the lowest temperatures the ^{11}B spin-lattice relaxation rate for EuB_6 is much larger than $T_1^{-1}$for the reference compound LaB_6. We associate this enhancement with excitations within the *f*-electron system. The observed strong temperature and field dependences of T_1^{-1} is typical for ferromagnets where the spin-lattice relaxation is well accounted for by the flipping of a nuclear spin inducing a magnon excitation, or vice versa.[17] To estimate the efficiency of the magnon-driven relaxation one needs detailed knowledge of the hyperfine interaction between the magnetic moments and the nuclear spins. As previously noted we assume that the interaction between the *f* electrons and the boron nuclei contains a transferred $\mathcal{H}_{\rm tr}$ and an electron-nucleus dipole $\mathcal{H}_{\rm dip}$ contribution. Thus the total hyperfine Hamiltonian may be written as

$$\mathcal{H}=\mathcal{H}_{\rm tr}+\mathcal{H}_{\rm dip}. \tag{13}$$

We mention here that if the crystal structure and the magnitude of the magnetic moment are known, $\mathcal{H}_{\rm dip}$ can easily be computed. For the transfer term the situation may be more complicated. If $\mathcal{H}_{\rm tr}$ does not have a simple isotropic form then a detailed account of this contribution is very difficult. However, since the hyperfine coupling enters only as an overall scaling factor in the relaxation, some qualitative information may still be obtained from the temperature and field dependences of T_1^{-1}.

The spin-wave approach, used for the analysis of the magnetization in Sec. III C can be applied here to estimate the spin-lattice relaxation rate at low temperatures $T \ll T_{\rm C}$. In this approach the spin operators S^+, S^-, and S_z are expanded in terms of boson operators $\mathbf{b}^\dagger$ and $\mathbf{b}$ for the creation and annihilation of a spin-wave excitation,[14] respectively. The first-order expansion in spin-wave operators corresponds to the one-magnon process where a nuclear spin flip is accompanied by the creation of a spin wave or vice versa. Usually this mechanism is forbidden because the energy is not conserved. The two-magnon or Raman process represents the situation of a spin wave with wave vector $\mathbf{k}$ being scattered into a new state $\mathbf{k}'$ by a nuclear spin-flip. In this case the energy is easily conserved but the condition of angular momentum conservation may prohibit this process. However, if the hyperfine Hamiltonian includes terms of the form $A^{[+z]}\cdot I^+ S_z$, the Raman process has a nonvanishing probability. The operator I^+ is the usual nuclear spin raising operator and $A^{[+z]}$ is the hyperfine matrix component associated with the term $I^+ S_z$, where S_z is the *z* component of the Eu $4f$-electron spin operator. Note that for Eu^{2+}, the total angular momentum $J=S=7/2$. The above form of the hyperfine Hamiltonian is expected in the presence of the dipole interaction or if the hyperfine transfer mechanism is anisotropic. In both cases the terms $I^+ S_z$ involve terms with one creation and one annihilation boson operator[14,18,19]

$$\mathcal{H}_{\rm hf}^{[+z]}=\frac{1}{2}A^{[+z]}I^+S_z=\frac{1}{2}A^{[+z]}I^+ \times\left[S-\frac{1}{N}\sum_{\mathbf{k},\mathbf{k}'}\exp[i(\mathbf{k}-\mathbf{k}')\cdot\mathbf{r}]\mathbf{b}_{\mathbf{k}}^\dagger\mathbf{b}_{\mathbf{k}'}\right], \tag{14}$$

and the two-magnon process is allowed. In Eq. (14), $\mathbf{r}$ represents the position of the spin. Using Fermi's golden rule the spin-lattice relaxation rate is of the form[18]

$$\frac{1}{T_1}=\frac{\pi(A^{[+z]})^2}{\hbar}\int n_\epsilon(1+n_\epsilon)D^2(\epsilon)d\epsilon, \tag{15}$$

where $D(\epsilon)$ represents the density of spin-wave states, ϵ is the energy associated with a spin-wave excitation given in Eqs. (8)–(10), and n_ϵ is the Bose-Einstein occupation factor $n_\epsilon \equiv [\exp(\epsilon/k_{\rm B}T)-1]^{-1}$. In addition to this first-order Raman process, a second-order two-magnon process, which does not require the conservation of the *z* component of the angular momentum, is mediated by the dipole interaction among ordered moments.[17] In an even higher-order expansion, three-magnon processes where the nuclear spin flip is associated with the annihilation of one and the creation of two spin waves, are encountered. In this case the energy and momentum conservation requirements can always be fulfilled and, therefore, this type of process is always allowed.

The solid lines in Fig. 12 represent calculations of $T_1^{-1}(T,H)$ for a two-magnon dominated relaxation process employing Eq. (15) and using $J_1=0.157$ K, $J_2=0$ and $\Delta=1.4$ K, one of the parameter sets discussed in Sec. III C. The hyperfine coupling constant $A^{[+z]}$ provides an overall free scaling parameter for obtaining the best agreement between our model calculations and the results of our measurements. The solid lines displayed in Fig. 12 were obtained with $A^{[+z]}S_z/\hbar\gamma_{11B}\approx 0.45$ T, with $S_z=7/2$. We note that with these exchange couplings J_1, J_2 and the energy gap Δ that we obtained via the analysis of the ^{153}Eu NMR spectra (see Fig. 8 and corresponding discussion) the salient features of the ^{11}B spin-lattice relaxation may be reproduced rather well. Using the same simple approximation for calculating $T_1^{-1}(T,H)$ with the second parameter set mentioned in Sec. III C, i.e., $J_1=0.063$ K, $J_2=0.063$ K, and $\Delta=0$ K, the agreement between calculation and experiment is distinctly worse. This confirms that the magnon excitation spectrum at low energies is dominated by a gap $E_g/k_{\rm B}$ of the order of 1 K. The nontrivial agreement between the calculated and the

observed temperature and field dependences of T_1^{-1} in the range where the spin-wave model ought to be applicable, gives strong evidence that the relaxation is indeed dominated by two-magnon processes and that our approximation captures the essential ingredients. At higher temperatures, where the deviations from the saturation magnetization grow substantially, we expect the spin-wave approximation to fail and higher-order processes to become more significant. Here we point out that, based on the results of previous electrical resistivity ρ measurements, a magnon gap of the order of 45 K has been suggested for EuB_6 (Ref. 7). Our analysis of the NMR data presented above finds no support for this claim. We, therefore, believe that the observed features of $\rho(T)$ have an origin different from the electron-magnon scattering assumed in Ref. 7.

We now turn our attention to the hyperfine coupling $A^{[+z]}$. As mentioned above the best agreement with the field and temperature dependences of the spin-lattice relaxation rate yields $A^{[+z]}S_z/\hbar\gamma_{11_B} \approx 0.45$ T. The two-magnon process is allowed only if the hyperfine interaction is anisotropic or if the electron and nuclear-spin quantization axes are not collinear. An anisotropic interaction involved in our situation is the direct electron-nucleus dipole interaction. The magnitude of $A^{[+z]}$, calculated for the dipole case for Eu moments aligned along the three directions [100], [110], and [111], is too small to quantitatively account for the magnitude of the measured spin-lattice relaxation rate. Other causes that might enhance $A^{[+z]}$ are a lattice distortion enhancing the dipole coupling, or an anisotropic hyperfine transferred interaction that invokes a hyperfine coupling $A^{[+z]}$ of the order of 0.45 T.

The measured temperature and field dependences of the ^{11}B spin-lattice relaxation rate are thus consistent with a two-magnon driven relaxation mechanism. The dipole interaction between the Eu moments and the B nuclei alone seems insufficient to quantitatively account for the observed value of T_1^{-1}. This deficit may hint to either an anisotropic transferred hyperfine interaction and/or a temperature-induced lattice distortion. Both the lattice distortion and/or the anisotropic transferred hyperfine interaction need to be consistent with the two inequivalent sites observed in the ^{11}B-NMR spectra and with the equal spin-lattice relaxation rates observed for both these sites.

IV. CONCLUSIONS

Our results for the ^{153}Eu-NMR spectra signal that below 2 K, well within the ferromagnetic state of EuB_6, slight changes in the electronic environments near the Eu sites provoke the gradual development of a second ordered phase. The small but distinct difference in the observed hyperfine fields of the two coexisting phases is of the order of 1% with no appreciable effect on the dynamics of magnon excitations. Since the results for the ^{11}B NMR give no hint for dramatic changes around 2 K, we have to conclude that the phase B detected in the results of ^{153}Eu NMR does not have very different electronic or magnetic properties than phase A, present already at higher temperatures. This in turn leads to the question of what causes two similar coexisting phases in EuB_6? It is natural to attribute the differences of these phases to weak terms in the electronic Hamiltonian which either violate an important symmetry, or which act only through a higher-order perturbation process. Spin-orbit and crystal-field interactions, acting weakly on the Eu^{2+} ions, are the prime candidates for such a mechanism. Their main role would not just be the lifting of the degeneracy of the $4f^7$ ground state, but to induce two slightly different ground states. In any case our findings point to a delicately balanced situation for the magnetic ground state of EuB_6.

The low-temperature ^{11}B-NMR spectra reveal two inequivalent B sites, experiencing different hyperfine fields. It is difficult to unequivocally identify the cause for this difference. None of the most obvious ferromagnetic alignments of the Eu moments can, by itself, explain both the magnitude and the difference of the hyperfine fields. Thus very small lattice distortions at low temperatures cannot be ruled out to be, at least partially, the cause for two inequivalent ^{11}B sites. Possible lattice distortions are of interest here in connection with electron-lattice interactions influencing the magnetic and transport properties of EuB_6. The similarity with manganese oxides where large magnetoresistive effects combined with ferromagnetic order and enhanced metallicity[20] are, at least partially ascribed to strong electron-lattice interactions,[21,22] is intriguing.

We have attempted to analyze our results on the ^{153}Eu line shift, induced by the spontaneous magnetization in the ferromagnetic phase, and of the ^{11}B spin-lattice relaxation well below the Curie temperature, by invoking the spin-wave theory of Holstein and Primakoff.[14] The experimental results are fairly well accounted for by a dominant two-magnon relaxation process and assuming a gap E_g in the magnon excitation spectrum such that E_g/k_B is of the order of one Kelvin. Finally we note that our microscopic measurements in externally applied magnetic fields give no evidence for a moment reorientation around 14 K, as has been suggested to occur in zero field in Ref. 7.

[1] B.T. Matthias, Phys. Lett. **27A**, 511 (1968).
[2] Z. Fisk, D.C. Johnston, B. Cornut, S. von Molnar, S. Oseroff, and R. Calvo, J. Appl. Phys. **50**, 1911 (1979).
[3] C.N. Guy, S. von Molnar, J. Etourneau, and Z. Fisk, Solid State Commun. **33**, 1055 (1980).
[4] S. Massida, A. Continenza, T.M. de Pascale, and R. Monnier, Z. Phys. B **102**, 83 (1997).
[5] W. Henggeler, H.R. Ott, D.P. Young, and Z. Fisk, Solid State Commun. **108**, 929 (1998).
[6] L. Degiorgi, E. Felder, H.R. Ott, J.L. Sarrao, and Z. Fisk, Phys. Rev. Lett. **79**, 5134 (1997).
[7] S. Süllow, I. Prasad, M.C. Aronson, J.L. Sarrao, Z. Fisk, D. Hristova, A.H. Lacerda, M.F. Hundley, A. Vigliante, and D. Gibbs, Phys. Rev. B **57**, 5860 (1998).
[8] J.C. Cooley, M.C. Aronson, J.L. Sarrao, and Z. Fisk, Phys. Rev. B **56**, 14 541 (1997).
[9] J.L. Gavilano, B. Ambrosini, P. Vonlanthen, H.R. Ott, D.P. Young, and Z. Fisk, Phys. Rev. Lett. **81**, 5648 (1998).

[10] H.R. Ott, B. Ambrosini, J.L. Gavilano, Z. Fisk, D.P. Young, M.E. Torelli, J.L. Sarrao, and J.D. Thompson (unpublished).
[11] H.R. Ott, M. Chernikov, E. Felder, L. Degiorgi, E.G. Moshopoulou, J.L. Sarrao, and Z. Fisk, Z. Phys. B **102**, 337 (1997).
[12] J. Barak, I. Siegelstein, A. Gabai, and N. Kaplan, Phys. Rev. B **8**, 5282 (1973).
[13] M.W. Pieper, J. Kötzler, and K. Nehrke, Phys. Rev. B **47**, 11 962 (1993).
[14] T. Holstein and H. Primakoff, Phys. Rev. **58**, 1098 (1940).
[15] W. Zinn, J. Magn. Magn. Mater. **3**, 23 (1976).
[16] D. Pushin (private communication).
[17] D. Beeman and P. Pincus, Phys. Rev. **166**, 359 (1968).
[18] J. Barak, A. Gabai, and N. Kaplan, Phys. Rev. B **9**, 4914 (1974).
[19] A.H. Mitchell, J. Chem. Phys. **27**, 17 (1957).
[20] Y. Tokura, Curr. Opin. Solid State Mater. Sci. **3**, 157 (1998).
[21] A.J. Millis, P.B. Littlewood, and B.I. Shraiman, Phys. Rev. Lett. **74**, 5144 (1995).
[22] A.J. Millis, B.I. Shraiman, and R. Mueller, Phys. Rev. Lett. **77**, 175 (1996).